VI. SOLID-STATE PHYSICS IN INTENSE MAGNETIC FIELDS

John A. Woollam

The Lewis Research Center has developed a number of very large magnets. These magnets are large, not only in available volume for experiments but also in magnetic field strength. This makes these magnets unique for solid-state physics experiments. Certain experiments, such as thermomagnetic effects, are easier to perform in large working volumes. Other experiments, such as extreme quantum limit studies and spin-orbit interaction studies, are possible only in high magnetic fields. Many of the solid-state experiments which are performed are devoted to understanding the physical nature of solids in fields and to searching for fundamentally new phenomena. Yet some of the experiments have practical purposes, such as determining how transistors perform in fields and how thermometers are affected by fields. This paper describes some of the physics experiments and some of the results which have engineering application. These include transport experiments, transistors in magnetic fields, magnetocaloric experiments, and a technique for plotting magnetic field lines in plasma containment magnets.

THE MAGNETS

Figure VI-1 shows a 4.0-tesla magnet (ref. 1) which produces a horizontal field with vertical probe access. It consists of superconducting wire wound on a 4-inch-diameter iron core. This produces a field directed out of the figure. The outside dimensions are 1 by 1 by 1 foot. The gap between pole faces is 1 inch. The dewar and magnet are precooled to 78 K by the surrounding liquid nitrogen dewar. Iron specific heat below 78 K is low enough that very little liquid helium is evaporated in cooling the magnet to 4 K and covering it with liquid. The solid to be studied is attached to a long probe and inserted from above. The magnet and sample are then at bath temperature which can be lowered from 4.2 to 1.2 K by pumping on the helium with a large vacuum pump. The sample can be rotated from above, changing the angle between the field and the crystal axis by a motor attached to the drive gear. Angles are recorded by an infinite-resolution, high-linearity potentiometer attached to the drive gear, and field strengths are measured by integrating the

voltage induced in a coil placed near the center of the field. This method of measuring field strength is accurate and independent of bath temperature, whereas, a magnetoresistor calibration depends on bath temperature. Integrator output is calibrated against nuclear magnetic proton resonances (NMR). Integrator drift is the biggest source of error for this method. The magnet takes 100 liquid liters of helium for about 10 hours of running at 4 K or about 6 hours at 1.2 K. The major advantages of this magnet for solid-state research are threefold. (1) The transverse field permits changing the angle between the field and the sample by rotating the probe from above. (In an axial access solenoid a gearing mechanism must be used.) (2) Helium consumption is low so that little time is spent transferring. (3) At low fields the iron core provides a highly homogeneous field. The superconducting coils provide a maximum field of about twice the field of a conventional electromagnet.

Figure VI-2 shows a 10.5-tesla superconducting solenoid. It has an insert dewar and sample probe as shown. The field is vertical and parallel to the access holes, so any rotation of the sample is done with gearing. Helium at 4.2 K covers the magnet, and an insert dewar pumpable to 1 K is large enough to take a 2-inch-diameter probe. This large dimension, plus high maximum field, gives the magnet advantages over the 4-tesla transverse magnet just described. The field strength in the 10.5-tesla magnet is measured with a copper magnetoresistor calibrated against NMR resonances at 4 K. Major disadvantages of this magnet are threefold. (1) After the magnet has been driven to 10 tesla, a field of about 0.4 tesla remains trapped with zero magnet current. (2) Because shorting strips are used for stabilization, the magnet sweeps at a maximum rate of 10 tesla per half hour. (3) At this fast sweep rate, helium must be retransferred every 3 to 4 hours.

The third magnet system, shown in figure VI-3, is a 20-tesla neon-cooled cryomagnet (ref. 1). The most obvious advantage of this magnet is the high magnetic field it produces. The 20-tesla system is nearly vibration free since cooling is by neon evaporation. The 2-inch-diameter working volume allows for a large experiment. Temperatures down to 1.3 K are possible. However, the insert dewar is long and narrow, so pumping to 1.3 K takes several hours. There are several other advantages of this magnet over the two described earlier. Rapid sweep rates are possible, which permits getting much information from the experiment in a short time. The field direction is easily reversed, and exact zero fields are available because remnant magnetizations are not present, as they sometimes are in superconducting solenoids. The field is highly homogeneous over large volumes. The major disadvantage of this magnet is that at slow sweep rates, only one run per day to maximum field is possible.

EXPERIMENTS INVOLVING TRANSPORT OF HEAT AND ELECTRICAL CURRENTS

Transport measurements provide a check on theoretical assumptions about the nature of solids and thus promote our understanding of these materials. They also provide a method of studying electron collisions. Coefficients such as the Hall effect are measured frequently to characterize the solid for its use in devices such as solid-state electronic elements. Figure VI-4 shows how a few of these coefficients are measured (ref. 2). On the left voltages V_1, V_2, and V_3 are the galvanomagnetic voltages developed when a current flows into the sample (where V_1 is the Hall voltage, V_2 is the transverse even voltage, and V_3 is the magnetoresistance voltage, all with a horizontal field, as shown). The measurement of thermomagnetic effects is described on the right side of figure VI-4. Heat flow is provided by a heater shown at the bottom of the sample. At the other end a heat sink is at the bath temperature. Because of the heat flow, voltages are produced in the sample. For constant heat currents, coefficient V_1 is proportional to the adiabatic Nernst-Ettingshausen coefficient, V_2 to the adiabatic thermal transverse even coefficient, and V_3 to the adiabatic thermoelectric coefficient, again, for the horizontal field, as shown.

As discussed earlier, experiments done in a superconducting solenoid with an axial field must have a gearing mechanism (fig. VI-5) in order to rotate the sample relative to the direction of the field (ref. 3). Two drive rods (fig. VI-5) are driven from above with synchronous motors. If the drive rods rotate in opposite directions, the apparatus tilts the sample, but does not rotate it about its cylinder axis. If the drive rods turn in the same direction, the sample will not tilt, but will rotate about its cylinder axis. This apparatus thus provides a rotation drive with two independent degrees of rotational freedom. This permits measuring transport coefficients in a solenoid for any angle between the field and the sample. Typical data runs consist of continuously monitoring the transport coefficient against field at a fixed angle, or against angle at a fixed field. The parts of the probes which move in fields are made of poor conducting materials to reduce eddy currents.

An example of a rotation at a fixed field of 10 tesla is shown in figure VI-6 for a crystal of tin at 4.2 K (ref. 4). As can be seen, the electrical resistivity is highly anisotropic with respect to the angle between the crystal axis and field direction. At a symmetry direction which is at an angle marked zero in the figure, the resistivity in a field of 10 teslas drops to nearly the zero field value. At 10° on either side of this minimum, the resistivity is approximately 10^5 times as large as the zero field resistivity. The half width of this particular notch is 4°. For

comparison, the output of a Hall probe is shown, and, as is well known, the half width of the output of a Hall probe is 120°. This high anisotropy of the resistance could be used as a very sensitive device for plotting the direction and magnitude of the magnetic field in magnetic bottles used for plasma confinement. The angle of the minimum in the resistivity gives the direction, and the value of the resistance just outside the minimum gives the magnitude of the field. This could be used to plot point by point the field and its direction throughout the volume of the magnet. Samples with all dimensions less than 1/8 inch could be used.

Further Results in Tin

Results of some thermomagnetic experiments in tin are shown in figure VI-7 (refs. 2 and 4). The sample is in a field of 3.3 teslas and at a temperature of 1.2 K. As can be seen, the thermal transverse even coefficient is very small and is within experimental error of being zero for all fields and all angles. However, the Nernst-Ettingshausen coefficient is very large and highly anisotropic with respect to the angle between the field and the crystalline axes. The field dependence of this coefficient has been studied, and, for example, at an angle of -60° (as shown in the fig. VI-7), the Nernst-Ettingshausen coefficient has both cubic and quadratic dependencies on field. This large field dependence demonstrates the importance of this coefficient in possible thermoelectric power devices.

One of the most exciting discoveries in tin was large oscillations in the thermoelectric voltage as a function of field strength (ref. 5). Figure VI-8 shows the thermoelectric power as a function of field from 1.4 to 2 teslas for a sample of tin at 1.2 K. The thermopower is oscillatory in field, and the oscillations grow in amplitude with field strength. Each peak was assigned an integer, and the value of the field was measured at each peak. Figure VI-9 shows that plotting these integers as a function of the reciprocal of the magnetic field corresponding to each integer results in a straight line. These oscillations are periodic in inverse field, and they result from a quantization of electron orbits in momentum space. A strong magnetic field causes the charged electrons to spiral in a circular motion in a plane perpendicular to the direction of the field. The radius of these circles, or the area encompassed by these paths must have quantized values. This is shown by the following equation:

$$A_N = \frac{2\pi eH}{ch} (N + \gamma) \qquad (1)$$

where A_N is the area in momentum space for an electron trajectory perpendicular to the magnetic field direction. The area A_N depends linearly on field strength H, and for a fixed field there are N quantized areas. The quantization is only in the plane perpendicular to the direction of the magnetic field. Parallel to the magnetic field there is no quantization. Thus, the equation showing the quantization for A_N, results in a series of concentric cylinders. If the thermopower is calculated knowing that the areas in momentum space must be quantized when high magnetic fields are present, the following expression for the thermopower S results (ref. 6):

$$S \propto \cos\left(\frac{2\pi F}{H} - \frac{\pi}{4}\right) \tag{2}$$

The thermopower with a frequency of F is oscillatory as a cosine function and periodic in 1/H. The frequency F is proportional to A, the extremeal cross sectional area of the Fermi surface. Figure VI-10 shows the Fermi surface for a case of free electrons. For free electrons, the Fermi surface is a sphere. The cylinders which were described are inside the Fermi surface and are parallel to the direction of the magnetic field (ref. 7). The radius or cross sectional areas of the cylinders are proportional to field strength. Thus, as the field increases, the cylinders radii increase also. As the outermost cylinder passes through the Fermi energy, the electrons on it redistribute onto other cylinders. Since thermopower, as well as other transport coefficients, depend on the density of electron states at the Fermi surface, this redistribution of electrons on the outer cylinder, as it passes through the Fermi energy, causes the oscillations which are observed. In real metals, such as tin, the Fermi surface is not a simple sphere; it can be broken up into many different parts and can be very complicated. This can cause superimposed oscillations, all periodic in 1/H, but having different frequency values.

Figure VI-11 shows an example of two heating frequencies in tin at 1.2 K. The magnetization of this sample is plotted as a function of the strength of the magnetic field. Oscillations in the magnetization are the deHaas-vanAlphen effect. Tin has a large number of deHaas-vanAlphen frequencies, all dependent on the angle between the field and the crystalline axes, as shown in figure VI-12 (ref. 8). Here, the deHaas-vanAlphen frequencies are plotted as the function of angle between the field and the crystal axes. For the field along the [001] axis, for example, there are 10 superimposed frequencies. These frequencies can be accurately measured (with an error of 0.1 percent or less). This essentially gives the energy band structure at the Fermi energy. Energy bands, of course, occur at all energies,

not just the Fermi energy. But these measurements give an accurate method of determining the band structure at particular points. This allows the band structure theorist to match his calculation to the highly accurate experimental values at the Fermi energy. It is the band structure at energies other than the Fermi energy which result in the optical properties, for example, of solids.

Very unusual effects occur in tin because of magnetic breakdown as shown in figure VI-13 (refs. 5 and 9). In this figure the thermoelectric power is plotted as a function of magnetic field for two different angles between the field and the crystalline axis. At 52.95° large oscillations in the thermopower are seen, but, less than 2° away, at 51.23° the oscillations are barely visible. An extensive study of the amplitude of the oscillations as a function of the angle between the field and the crystalline axes has been made. Figure VI-14 shows the amplitude of the oscillations plotted against angle in the (110) rotation plane (ref. 5). As seen, there are several giant resonances in the amplitude. The two peaks near the [001] axis (at about $\pm 4^{\circ}$) are due to a linear chain of orbits which are opened and closed by magnetic breakdown. The resonances at A and A' are due to a coupling between two linear chains of orbits opened by magnetic breakdown. The exact mechanisms for the resonances B and B' and C and C' are not known, but they are believed also to be due to magnetic breakdown. The linear chain responsible for the resonances at $\pm 4^{\circ}$ are shown in figure VI-15. The large orbits $4a\zeta$ and the small orbits 3δ are not connected at zero field or very low field. At high fields magnetic breakdown probability increases, and the orbits 3δ and $4a\zeta$ can be connected. The probability for breakdown increases exponentially with the strength of the magnetic field, and the giant resonances in the amplitude of the thermopower oscillations are due to the opening and closing of orbits along the [110] direction, which is formed by a linear chain of the $4a\zeta$ and 3δ orbits (ref. 10).

The quantum phenomena described yield accurate information on the energy band structure of the solid. This gives the band structure at the Fermi energy and allows the theorist to construct an accurate band structure picture at all energies. Quantum phenomena also yield information about the effective masses of electrons, electron energies, and scattering mechanisms. Magnetic breakdown is seen especially well in the quantum phenomena in the galvanomagnetic and thermomagnetic effects.

Results in Graphite

In crystalline form, graphite is a highly anisotropic material. It is a semimetal, but, with alkali metals dissolved in it, it becomes a superconductor. In

one direction the crystal can be pulled apart with a piece of tape, and in the other, it has a tensile strength of over 100 000 psi. Fiber mats are now being made with this material; the mats are extremely strong and light and have been used in such things as airplane wings. Good synthetic crystals have only been available recently, so little is known about their transport properties in extremely high magnetic fields. One of these properties is the electrical magnetoresistance. In figure VI-16 we show the magnetoresistance of two different crystals of graphite as a function of field. The plots were made for two different temperatures for each crystal. These crystals are made by pressure annealing pyrolytic graphite at temperatures above 3300 K. Sample PG3 was annealed at a lower temperature and with less pressure than sample PG5. Thus, the crystallites are more highly oriented in sample PG5 than they are for PG3.

We've been studying the field and temperature dependence of various samples of pressure-annealed pyrolytic graphite in the extreme quantum limit. By "extreme quantum limit," we mean that there is only one Landau level beneath the Fermi energy for fields above approximately 8 teslas. As shown in figure VI-16, below 8 teslas the quantum resonances in the magnetoresistance are apparent and are stronger for the more highly oriented crystalline material. We've also been studying quantum resonances in the thermoelectric power as shown in figure VI-17 where the adiabatic thermoelectric power is plotted as a function of magnetic field from zero to about 3.8 teslas. At low fields there are sinusoidal oscillations due to quantization as was described earlier; however, at higher fields (above approx. 0.7 tesla) resonances result as each Landau level cylinder passes through the Fermi surface. With the sign of the resonances and their deHaas-vanAlphen frequency known, the position of the Fermi surface in the Brillouin zone, from which they originate, was determined.

Transistors in Fields

Of practical importance, is the study which we have been making of transistor performance in high magnetic fields. Table VI-1 lists several different materials of different constructions and their performance in a magnetic field (ref. 11). "Performance" is defined as the ratio of the gain of the transistor in the field, to the gain in zero field. The high field data listed were taken at 7 teslas, and the effects are very large. For example, in the npn-germanium alloy transistor, gain has been reduced to 27 percent of its value in zero field. The conclusions from this work are that planar diffused silicon transistors are best for use in magnetic fields. It is

also best to have the magnetic field oriented parallel to the carrier motion. Transistor performance is independent of whether the transistor is a pnp or an npn type.

MAGNETOCALORIC EXPERIMENTS

A second major class of experiments is magnetocaloric experiments. A schematic of the apparatus and the measuring electronics is shown in figure VI-18. The sample is thermally isolated by a carbon support rod. The sample sits in a vacuum, and the vacuum can is surrounded by liquid helium. Thus, the sample comes to an equilibrium temperature with the surrounding bath. The bath temperature varies from 4 to 1.0 K in most cases. The temperature of the sample is monitored with a carbon thermometer using an alternating-current Wheatstone bridge. The bridge consist of an oscillator driving the bridge, and off-balance is detected with the output of a phase sensitive detector, which is tuned to the oscillator frequency. Using this method, changes in the temperature of the sample on the order of 10^{-6} K can be detected. An example of this type of experiment is shown in figure VI-19, where the temperature of the sample is monitored as a function of field strength for a crystal of tin at 1.0 K and for fields between 2.3 and 5 teslas. Temperature changes are on the order of a few times 10^{-5} K, and the oscillations are a result of the quantization of electron orbits as was described earlier. These experiments yield information about the electron energy bands of the solid. The advantage of this method is that the samples need not be shaped. This method for studying quantum effects in solids is sensitive to spin-orbit coupling in the material. Measurements of the spin-orbit coupling in bismuth and antimony have been made by other observers (ref. 12). Preparations are underway to use this method on samples of lead telluride. The magnetocaloric method has been used in a preliminary test to study flux jumping in type II superconductors.

A third example of this type of experiment is the magnetic phases of cesium-manganese-chloride. Figure VI-20 shows the phase diagram for cesium-manganese-chloride material (ref. 13). The magnetic field strength is plotted as a function of the temperature of the sample. Above 5 K the sample is in a paramagnetic state. Below 5 K, in low fields, the sample orders antiferromagnetically. On raising the field at temperatures below 5 K, the spins of the sample flop 90^{o}. This figure was made for the field along one particular axis of the crystal. Studies of the magnetic phases of this crystal for other orientations at low field were made by other researchers. Other experimental methods, such as nuclear magnetic resonance were also used. In a sample of cesium-copper-chloride, the phase boundary between the antiferromagnetic region and the paramagnetic region becomes

pendent of temperature at a field of 6.2 teslas. The sample, starting at 1.2 K, cooled rapidly in an increasing field in the antiferromagnetic region and passed through the antiferromagnetic boundary into the paramagnetic region at a temperature of about 0.8 K and at a field of 6.2 teslas. On increasing the field in the paramagnetic state, the sample warms very rapidly. From the value of the field at which rapid cooling of the sample changed to rapid heating of the sample, we are able to detect the upper antiferromagnetic - paramagnetic boundary. Low temperatures have traditionally been achieved by adiabatically demagnetizing a paramagnetic material. The rapid cooling which occurs in the antiferromagnetic region in an increasing field for cesium-copper-chloride, for example, opens the possibility for experiments at low temperatures in increasing fields.

Other experiments being performed at Lewis are, for example, magnetostriction experiments in bismuth, lead telluride, and copper (ref. 14); flux flow and flux pinning experiments in thin film superconductors (ref. 15); and studies of the critical field, critical current, and critical temperature for superconducting alloys that are used for constructing superconducting magnets (ref. 16). These experiments are continuing.

REFERENCES

1. Laurence, James C.: High-Field Electromagnets at NASA Lewis Research Center. NASA TN D-4910, 1968.

2. Woollam, John A.: Galvanomagnetic and Thermomagnetic Effects in White Tin in Fields to 3.3 Tesla and at Temperatures between 1.2 and 4.2 K. NASA TN D-5227, 1969.

3. Brennert, G. F.; Reed, W. A.; and Fawcett, E.: Low Temperature Sample Holder Providing Two Degrees of Freedom in a Solenoid. Rev. Sci. Instr., vol. 36, no. 8, Aug. 1965, pp. 1267-1269.

4. Woollam, John A.: Thermomagnetic Effects and Fermi Surface Topology: Results in Metallic Tin at Low Temperatures. Presented at the Am. Phys. Soc. Winter Meeting, San Diego, Calif., Dec. 18-20, 1968.

5. Woollam, John A.; and Schroeder, P. A.: Magnetic Breakdown and Thermoelectricity in Metallic Tin. Phys. Rev. Letters, vol. 21, no. 2, July 8, 1968, pp. 81-82.

6. Guseva, G. I.; and Zyryanov, P. S.: Quantum Theory of Thermomagnetic Phenomena in Metals and Semiconductors. Phys. Stat. Solidi, vol. 8, 1965, pp. 759-772.

7. Chambers, R. G.: Our Knowledge of the Fermi Surface. Can. J. Phys., vol. 34, no. 12A, Dec. 1956, pp. 1395-1423.

8. Craven, J. E.; and Stark, R. W.: de Haas-van Alphen Effect and Fermi Surface of White Tin. Phys. Rev., vol. 168, no. 3, Apr. 15, 1968, pp. 849-858.

9. Woollam, J. A.: Anomalous Shubnikov-de Haas Amplitudes in White Tin. Phys. Letters, vol. 27A, no. 4, July 1, 1968, pp. 246-247.

10. Young, R. C.: Magnetoresistance and Coupled Orbits in Tin. Phys. Rev., vol. 152, no. 2, Dec. 9, 1966, pp. 659-660.

11. Hudson, Wayne R.; Meyn, Erwin H.; and Schultz, Clarence W.: Transistor Performance in Intense Magnetic Fields. NASA TN D-5428, 1969.

12. McCombe, B.; and Seidel, G.: Magnetothermal Oscillations and Spin Splitting in Bismuth and Antimony. Phys. Rev., vol. 155, no. 3, Mar. 15, 1967, pp. 633-641.

13. Butterworth, G. J.; and Woollam, J. A.: Magnetic Phase Diagram of $CsMnCl_3 \cdot 2H_2O$. Phys. Letters, vol. 29A, no. 5, May 19, 1969, pp. 259-260.

14. Aron, P. R.; and Chandrasekhar, B. S.: Oscillatory Magnetostriction and Deformation Potentials in Bismuth. Phys. Letters, vol. 30A, no. 2, Sept. 22, 1969, pp. 86-87.

15. Hudson, Wayne R.; and Jirberg, Russell J.: Nonlinear Flux Flow in Single Crystal Niobium. NASA TN D-5198, 1969.

16. Aron, P. R.; and Ahlgren, G. W.: Critical Surfaces for Commercial Nb_3Sn Ribbon and Nb - 25% Zr Wire. Advances in Cryogenic Engineering. Vol. 13. K. D. Timmerhaus, ed., Plenum Press, 1968, pp. 21-29.

TABLE VI-1. - TRANSISTOR PERFORMANCE IN MAGNETIC FIELD

Material	Material type	Construction	Relative performance at 7.0 T (70 kG)
Silicon	pnp	Alloy	0.83
Germanium	npn	Alloy	.31
Silicon	↓	Planar diffused	.96
Germanium	↓	Alloy	.27
Silicon	↓	Planar diffused	.94
Silicon	pnp	Planar diffused	.94
Germanium	pnp	Planar diffused	.67

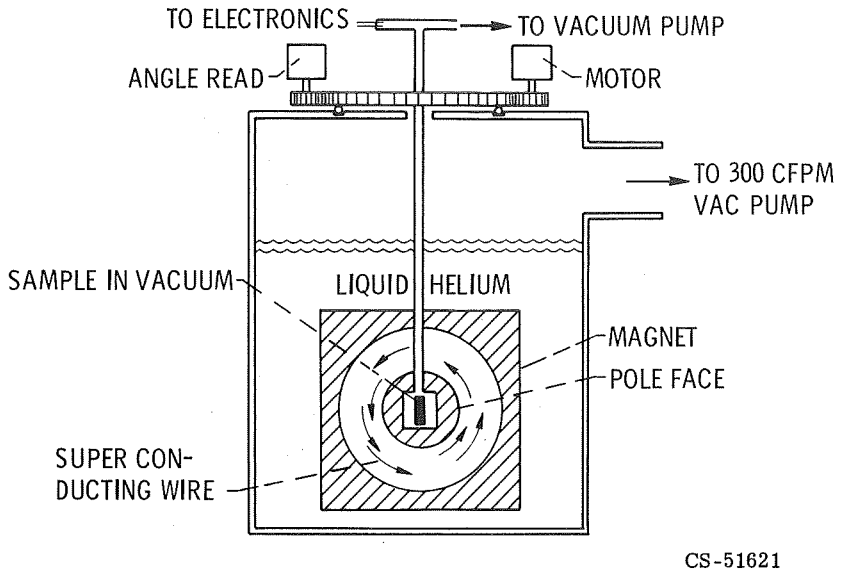

Figure VI-1. - 4.0-Tesla transverse field magnet.

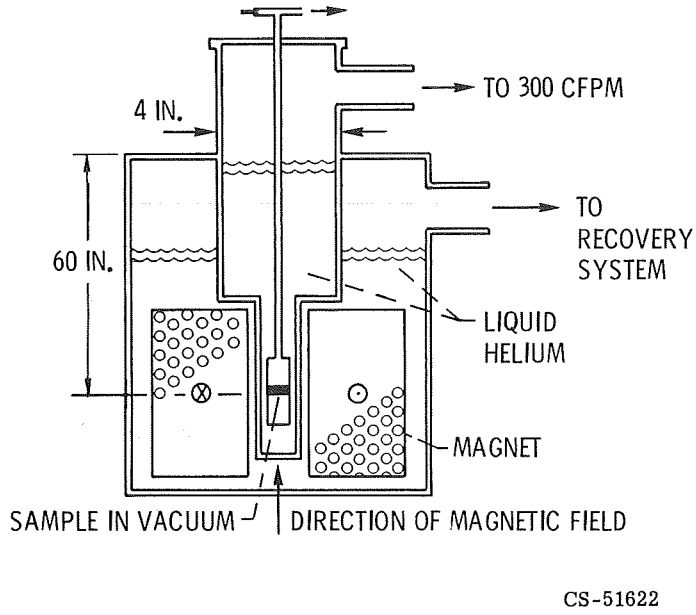

Figure VI-2. - 10.5-Tesla superconducting solenoid.

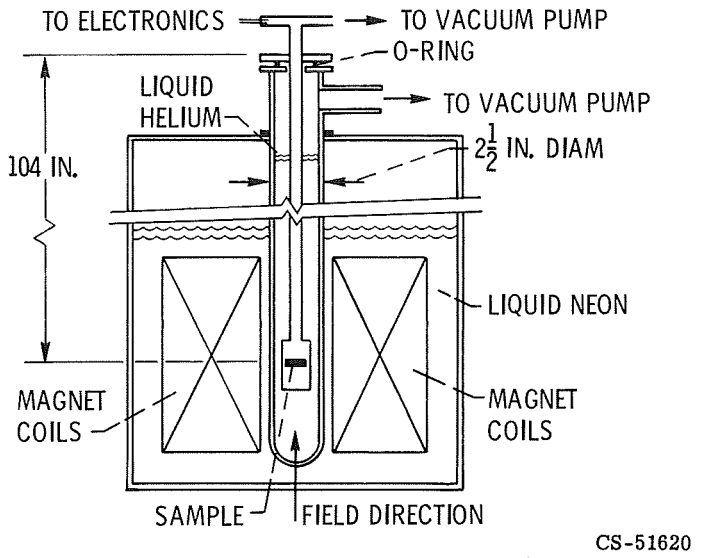

Figure VI-3. - 20-Tesla neon-cooled cryomagnet.

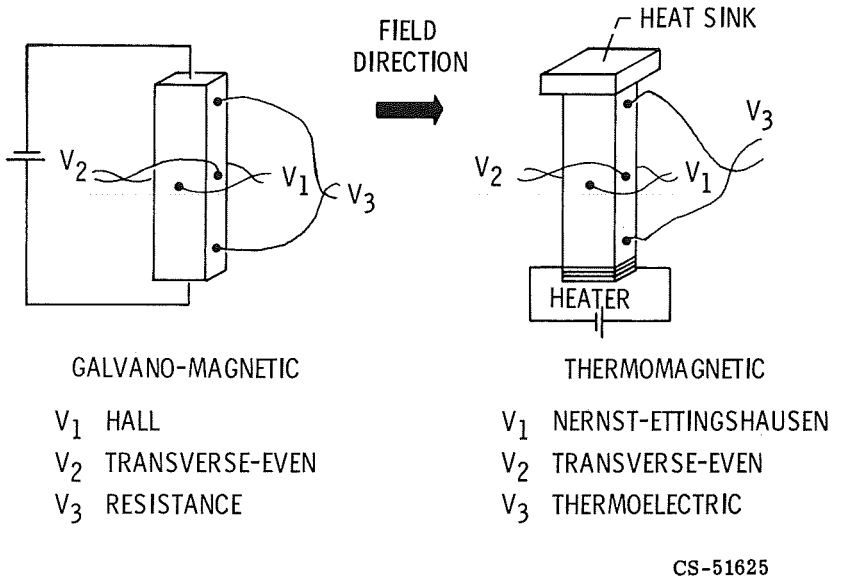

Figure VI-4. - Transport coefficients.

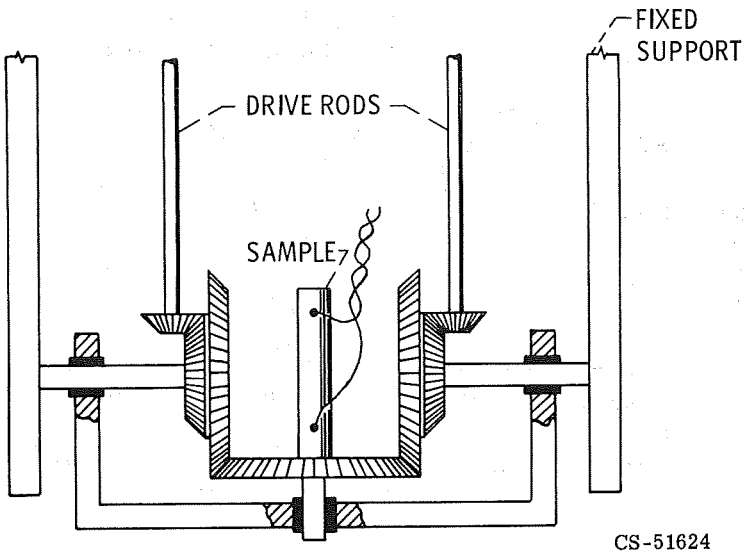

Figure VI-5. - Superconducting solenoid gearing mechanism for rotating or tilting the sample.

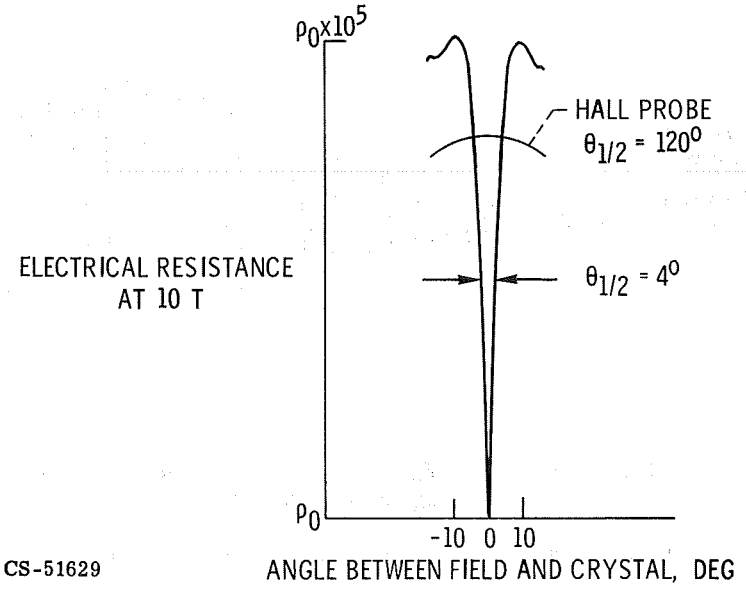

Figure VI-6. - Tin at 4.2 K.

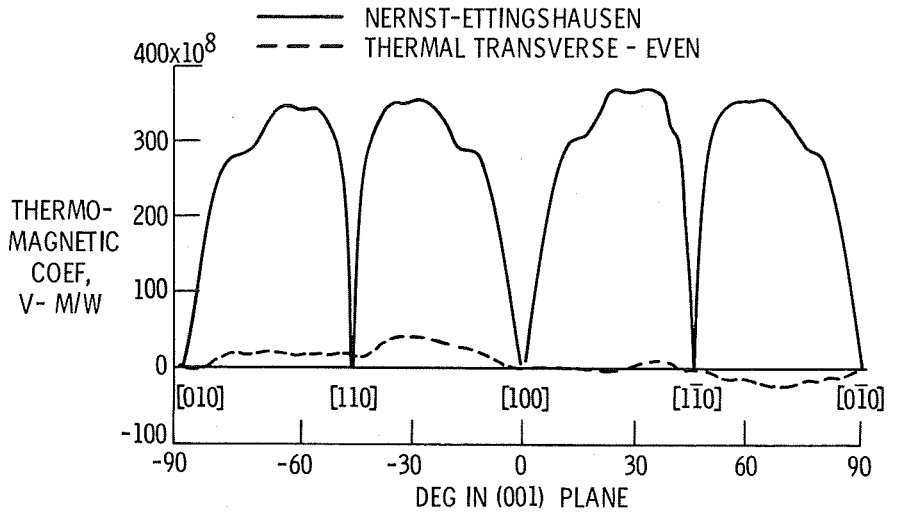

Figure VI-7. - Tin; field, 3.3 teslas; temperature, 1.2 K.

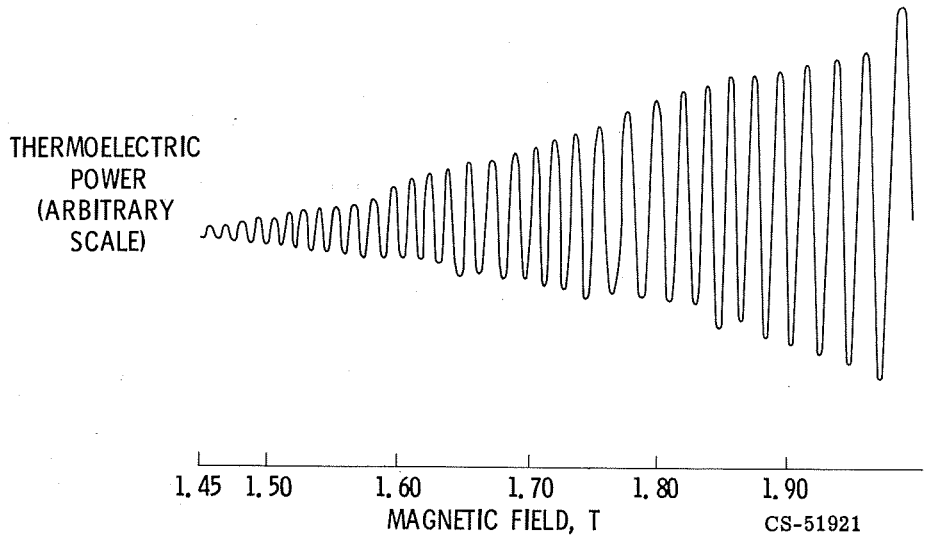

Figure VI-8. - Thermoelectric quantum effects in tin at 1.2 K.

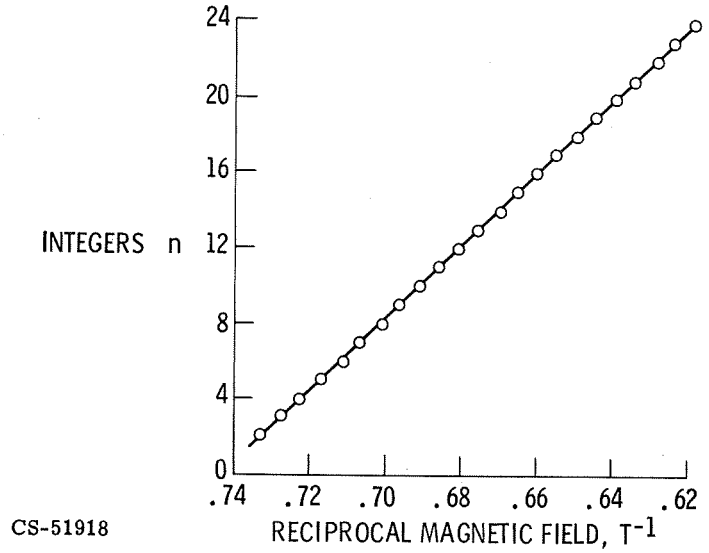

Figure VI-9. - Demonstration of periodicity in inverse field.

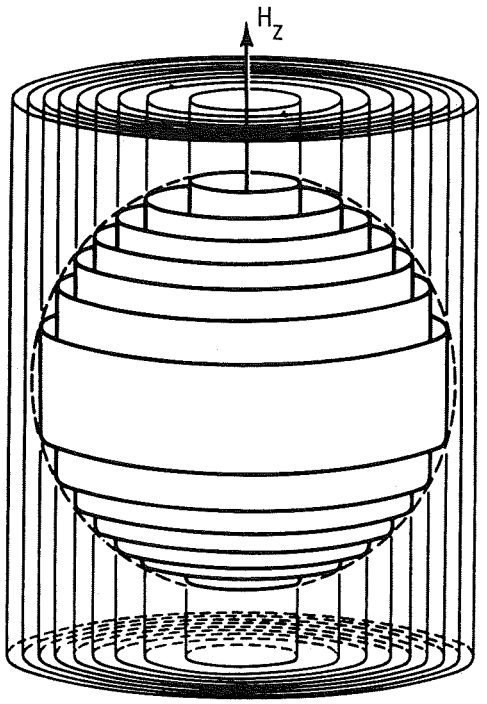

Figure VI-10. - Quantization of energy spectrum in x-y plane into discrete cylindrical surfaces in k-space under influence of applied magnetic field H_z (after Chambers, 1956).

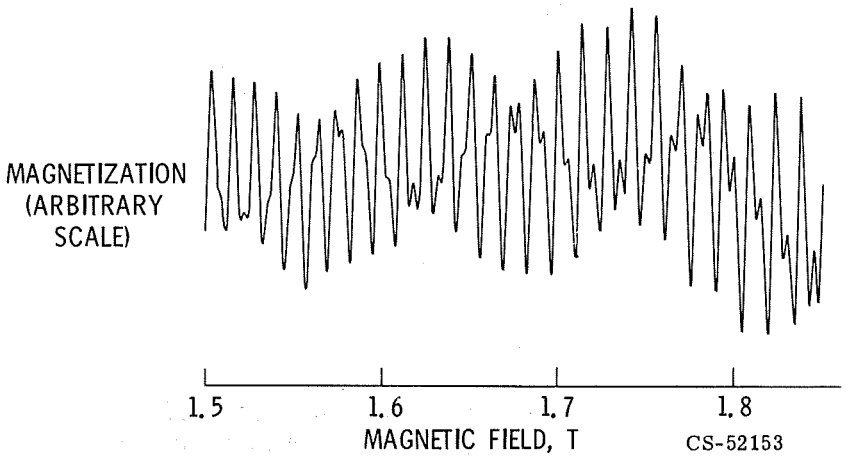

Figure VI-11. - deHaas-vanAlphen effect in tin at 1.2 K. Two beating frequencies shown.

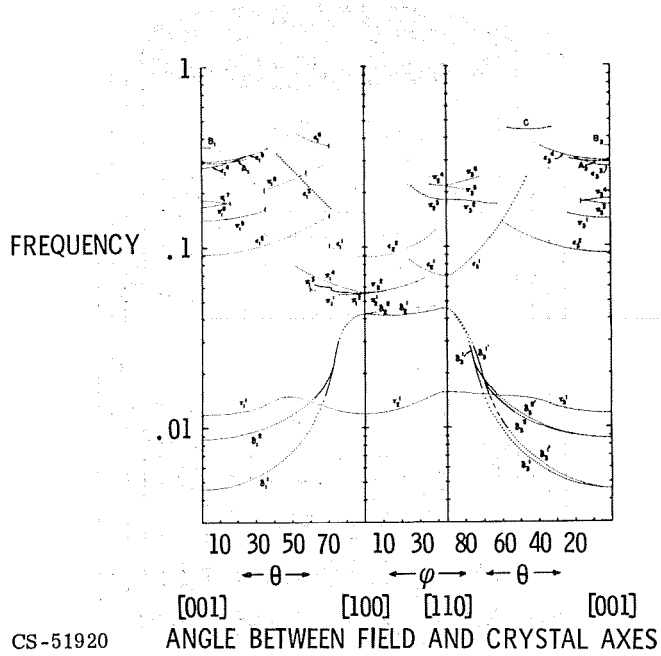

Figure VI-12. - deHaas-vanAlphen frequencies for tin (after Craven and Stark).

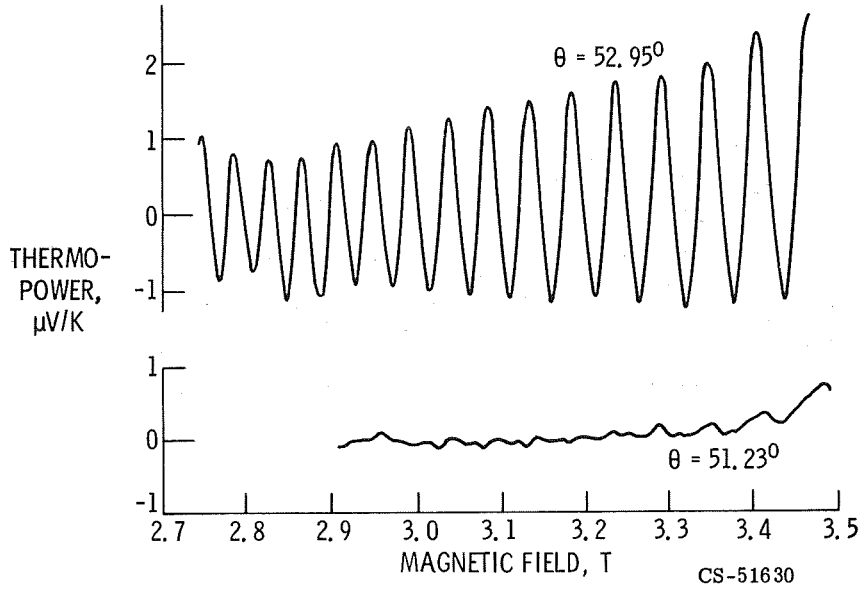

Figure VI-13. - Tin magnetic breakdown at 4.2 K.

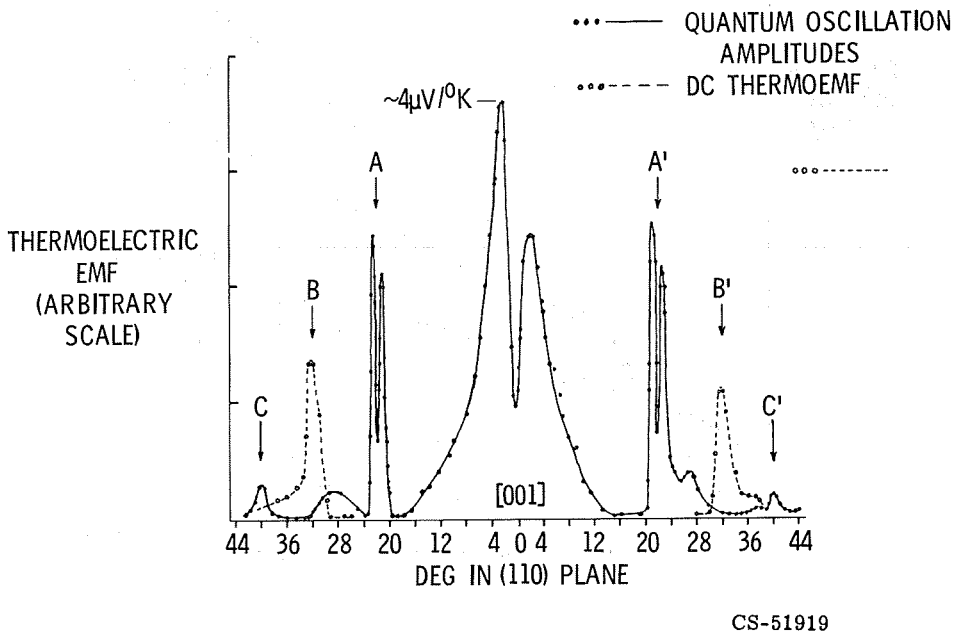

Figure VI-14. - Magnetic breakdown in tin; field strength, 3.3 teslas; temperature, 1.2 K.

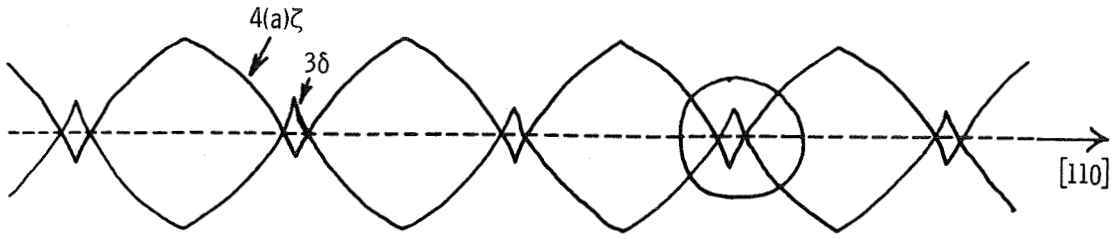

Figure VI-15. - Linear chain of orbits connected by magnetic breakdown.

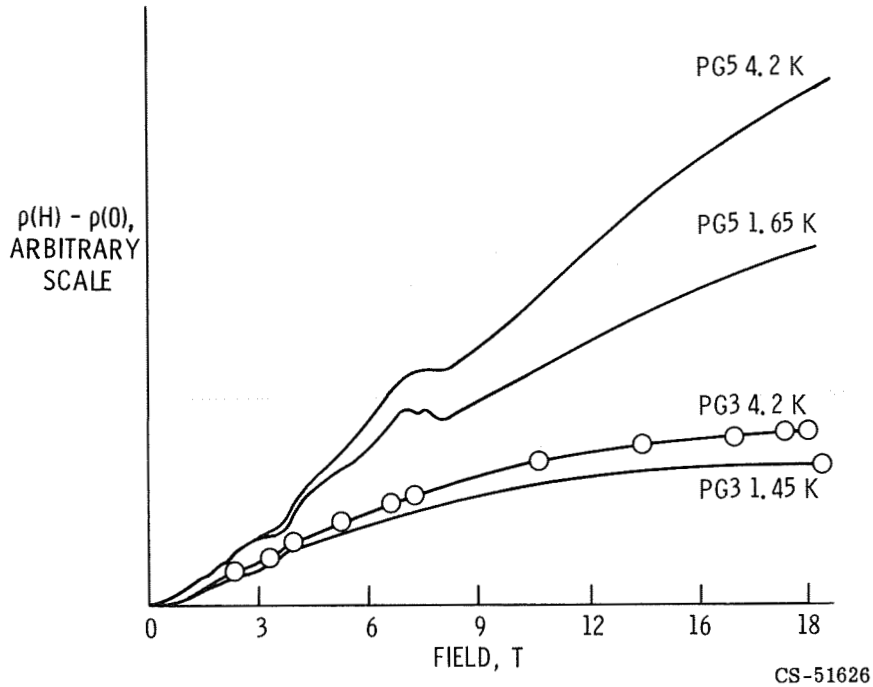

Figure VI-16. - Magnetoresistance of graphite.

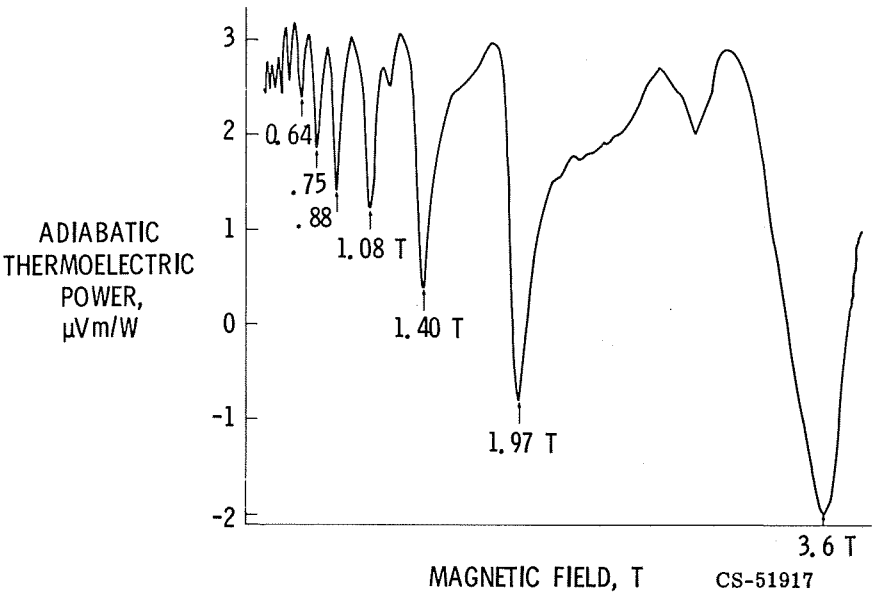

Figure VI-17. - Graphite quantum resonances at 1.1 K.

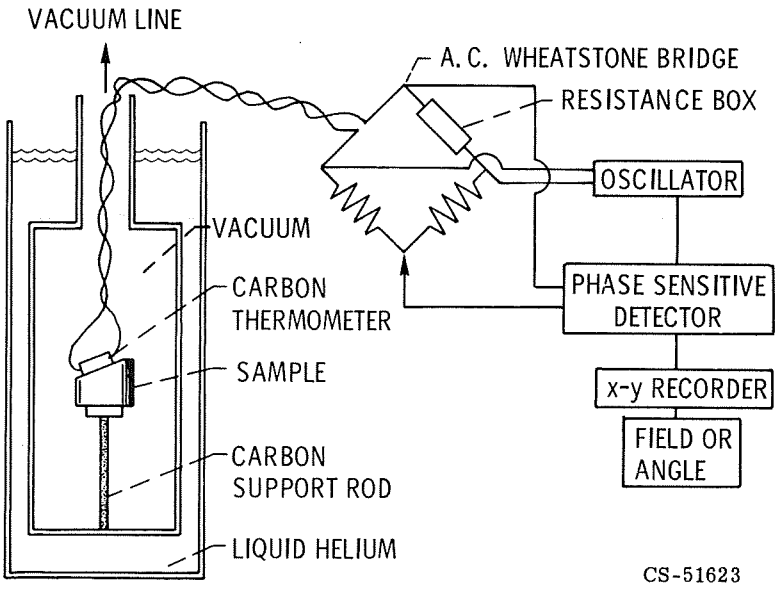

Figure VI-18. - Magnetocaloric experiments.

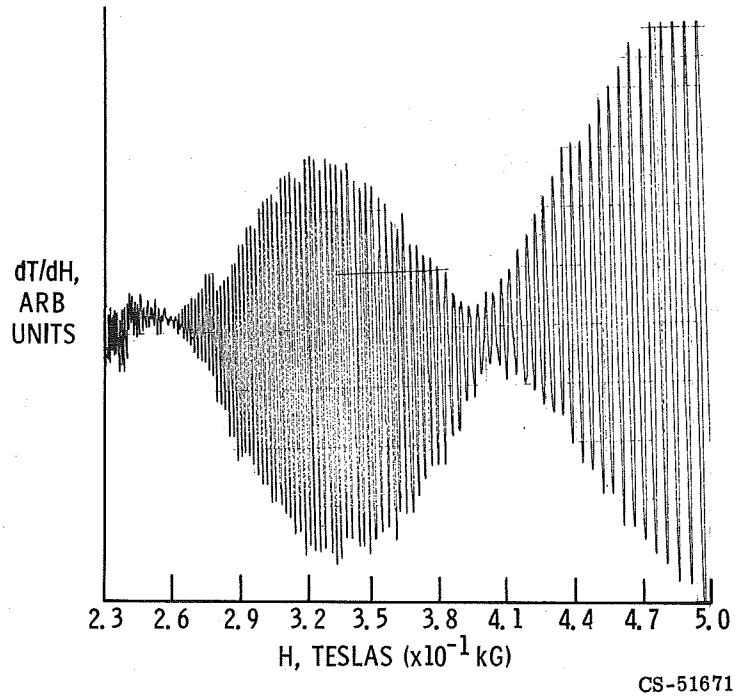

Figure VI-19. - Tin at 1.0 K.

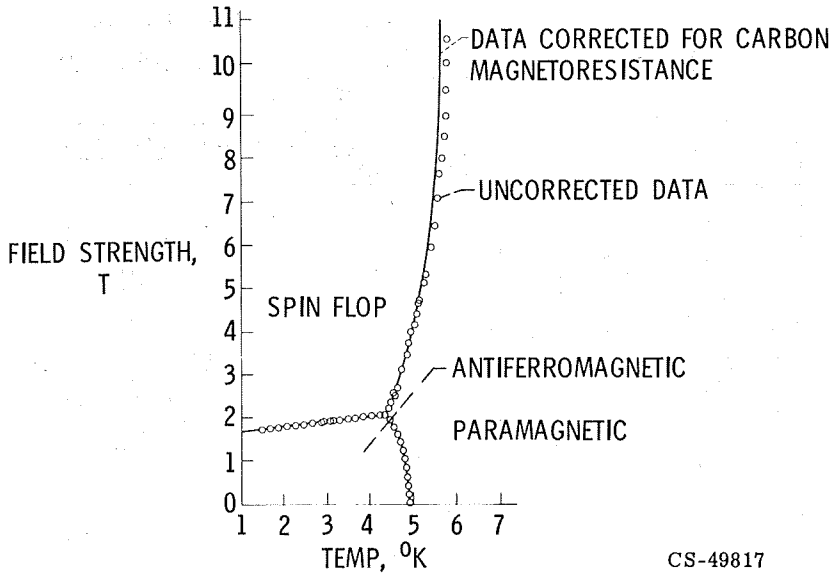

Figure VI-20. - Magnetic phases of $CsMnCl_3 \cdot 2H_2O$.